

Weakening of $N = 28$ shell gap and the nature of 0_2^+ states

Bhoomika Maheshwari*

Department of Physics, Faculty of Science, University of Zagreb, Zagreb, HR-10000, Croatia

E-mail: bhoomika.physics@gmail.com

*:Corresponding author

Kosuke Nomura

Department of Physics, Hokkaido University, Sapporo 060-0810, Japan

Nuclear Reaction Data Center, Hokkaido University, Sapporo 060-0810, Japan

E-mail: nomura@sci.hokudai.ac.jp

Abstract. The work reports a novel application of the interacting boson model in light-mass region around ^{48}Ca , that takes into account intruder states and configuration mixing. The model is shown to provide a reasonable description of the observed low-lying yrast and yrare states of the $N = 28$ even-even isotones from Si to Fe, and even-even Ca isotopes. The nature of 0_2^+ states is addressed in terms of the competition between spherical and deformed intruder configurations, and the rigidity of the $N = 28$ shell gap is tested, particularly for ^{44}S . The 0_2^+ isomer in ^{44}S is shown to arise from a weak mixing between the two configurations and called as shape isomer. The unresolved low-lying spectra in ^{46}Ar is also approached using the core-excitations across $N = 28$ shell. The $\text{SU}(3)$ structure in ^{42}Si is supported by the present calculation. The nearly spherical nature of ^{50}Ti , ^{52}Cr , ^{54}Fe and $^{42,44,46}\text{Ca}$ isotopes is found, while the core excitations are found to be essential for the description of yrare states. Shell model calculation is also performed for comparison.

1. Introduction

The atomic nuclei, as well as atoms, exhibit a few regular shell gaps, which give rise to extra stability. The concept of shell gaps for protons and neutrons at magic numbers stands as the backbone of modeling nuclear structure. The magic numbers emerge from the strong spin-orbit interaction, which is responsible for the extra binding of nucleons in orbitals having angular momentum aligned with their intrinsic spin [1]. These gaps are usually large enough to prevent excitations, but in lighter nuclei, nucleonic excitations across the magic-core are more likely to happen due to smaller shell gaps between the low- j orbitals [2], such as the very low energy of the first 2^+ state in ^{42}Si [3]. This

jeopardizes the conventional shell gaps and related shell model explanation of the low-lying excitations using a single nucleon or a pair of nucleons occupying just a few valence single-particle orbitals above the Fermi surface, even for semi-magic nuclei.

Variation of shell gaps with respect to proton-neutron asymmetry appears according to the underlying nuclear force [4]. The weakening of shell gaps can support deformed shapes in lighter semi-magic nuclei, also resulting in shape coexistence [2], such as in ^{44}S [7, 6, 5]. The presence of the 2.6 μs 0_2^+ isomer in ^{44}S , lying very close in energy to the 2_1^+ state, can be manifested using the core excitation across the $N = 28$ shell gap [7]. No such low-lying 0_2^+ isomer is known in the neighboring nucleus ^{46}Ar [8]. Both experimentally and theoretically, interpretation of those $N = 28$ isotones below ^{48}Ca , from ^{46}Ar to ^{44}S , and to ^{42}Si , is rather controversial and posed as a formidable challenge [3, 5, 6, 9]. The weakening of the $N = 28$ shell closure (i.e. closely lying $f_{7/2}$ and $p_{3/2}$ orbitals), and the resulting quadrupole correlations can reinforce deformation. This mechanism is interpreted within the quasi-SU(3) scheme [10], leading to quasi-degeneracy of the 2_1^+ and 0_2^+ states, which can be also viewed as a nuclear Jahn-Teller effect [11]. On the other hand, for those $N = 28$ isotones with the $f_{7/2}$ orbital occupied by valence protons, such as ^{50}Ti , ^{52}Cr , and ^{54}Fe , the yrare 0_2^+ state is also found, but not as an isomer, mainly because of the large difference between the excitation energies of the yrare 0_2^+ state and the yrast 2_1^+ state. These $N = 28$ isotonic nuclei with active $f_{7/2}$ orbital are usually adopted to be nearly spherical [12, 13], supporting the yrast 6^+ isomers [14]. But a weak second minimum on the potential energy surface was also reported [15, 16, 17], which is most likely responsible for yrare states. The similar is true for $^{42,44,46}\text{Ca}$ isotopes, with $\nu f_{7/2}$ being active.

In this article, we address the controversial cases of ^{42}Si , ^{44}S and ^{46}Ar using the interacting boson model (IBM) that incorporates the intruder states and configuration mixing. To the best of our knowledge, that extension of the IBM, referred hereafter as the IBM-CM [19], has not so far been considered in these light nuclei. We further compare the results for ^{50}Ti , ^{52}Cr , and ^{54}Fe , even-even $N = 28$ isotones beyond ^{48}Ca having protons in the fp shells, to the $^{42,44,46}\text{Ca}$ isotopes having neutrons in fp shells. This study also refers to the questionable double magicity of ^{48}Ca using the bosonic description of $N = 28$ isotones and compares to the fermionic wave functions calculated with the nuclear shell model (NSM). The detailed shell effects and seniority states such as the ones observed in the light nuclei in question have been considered beyond the reach of the conventional IBM framework including the one employed here, since it is built on the limited model space of low-spin pairs of valence nucleons only. The scope of this work is to test whether the IBM-CM with the parameters fine tuned to the observed data reproduces the energy level schemes and transition properties of the light mass nuclei where seniority-type configurations are supposed to play a dominant role. This study sheds light on the isomerism from the point of view of the IBM-CM, which has rarely been applied to that nuclear property.

The paper is organized as follows. In Sec. 2 we describe the IBM-CM framework and procedure to fix its parameters. In Sec. 3 the results of the IBM-CM calculations on the

energy levels and transition properties are discussed in comparison to the experimental data, and to the NSM calculations. Section 4 gives a summary and concluding remarks.

2. Formalism

The interacting boson model (IBM) [20] has been among the most successful and employed nuclear structure models together with the nuclear shell model [1], and the geometric collective model [21]. The IBM is comprised of s and d bosons with angular momenta 0^+ and 2^+ , representing the monopole and quadrupole pairs of valence nucleons, respectively [22, 23]. The number of bosons, $n = n_s + n_d$, is fixed by the microscopic interpretation of active valence nucleons $n = n_\pi + n_\nu$, where $n_\pi(n_\nu)$ equals the number of proton (neutron) particle or hole pairs counted from the nearest closed shell. A remarkable feature of the IBM is that it furnishes the algebra $U(6)$ with generators formed by a s and d_μ ($\mu = 0, \pm 1, \pm 2$) bosons. The $U(6)$ algebra is further reduced to $U(5)$, $SU(3)$ and $SO(6)$ subalgebras, providing the vibrational, rotational and γ -unstable spectra, respectively. The following IBM Hamiltonian has been shown to be adequate for phenomenological descriptions of the nuclear low-lying states.

$$\hat{H} = \epsilon \hat{n}_d + a_1 \hat{L} \cdot \hat{L} + a_2 \hat{Q} \cdot \hat{Q} , \quad (1)$$

where ϵ stands for single d -boson energy relative to that of s bosons. $\hat{n}_d = d^\dagger \cdot \tilde{d}$ is the d -boson number operator, with $\tilde{d}_\mu = (-1)^\mu d_{-\mu}$, $U(5)$ Casimir operator. The second term with the strength a_1 represents the $O(3)$ Casimir operator, with $\hat{L} = \sqrt{10}[d^\dagger \times \tilde{d}]^{(1)}$. The third term is the quadrupole-quadrupole interaction with the strength a_2 inducing the quadrupole deformation. The corresponding operator reads, $\hat{Q} = s^\dagger \tilde{d} + d^\dagger \tilde{s} + \chi [d^\dagger \times \tilde{d}]^{(2)}$, where χ is a parameter that determines the prolate ($\chi < 0$) or oblate ($\chi > 0$) deformation, reflecting the structure of collective nucleon pairs as well as the number of valence nucleons [22].

Configuration mixing is incorporated in such a way [24] that several independent (unperturbed) IBM Hamiltonians for the n , $n + 2$, $n + 4$, ... boson systems that are associated with the 0p-0h, 2p-2h, 4p-4h, ... particle-hole excitations, respectively, are introduced and are allowed to be mixed. Here we consider up to two configurations, i.e., normal $[n]$ and intruder $[n + 2]$ configurations, for which we assume for ^{44}S the vibrational $U(5)$ (with $\chi = 0$) and prolate deformed $SU(3)$ (with $\chi = -1.33$) symmetries, respectively. We further assume the normal $[n]$ space of ^{42}Si to be dominated by the $\overline{SU(3)}$ (with $\chi = 1.33$) symmetry, associated with the oblate deformation (see e.g., Ref. [25]). The full (IBM-CM) Hamiltonian reads,

$$\hat{H}' = \hat{H}_n + (\hat{H}_{n+2} + \Delta) + \hat{V}_{mix} , \quad (2)$$

where \hat{H}_n and \hat{H}_{n+2} represent unperturbed Hamiltonians for the normal (0p-0h) and intruder (2p-2h) boson spaces, respectively, and each has the form given by Eq. (1). Δ represents the energy needed to promote one nucleon pair from a major oscillator shell to the next. The last term is the interaction that admixes different boson spaces, and

is given by

$$\hat{V}_{mix} = \alpha(s^\dagger s^\dagger + ss)^{(0)} + \beta(d^\dagger d^\dagger + \tilde{d}\tilde{d})^{(0)}, \quad (3)$$

with α and β being mixing strength. The Hamiltonian (2) is diagonalized in the space $[n] \oplus [n+2]$ to obtain excitation energies and wave functions. The parameters used in the present IBM-CM calculations are listed in Table 1. The $E2$ operator is written as $\hat{T}(E2) = e_{2,n}\hat{Q}_n + e_{2,n+2}\hat{Q}_{n+2}$ with $e_{2,n}$ ($e_{2,n+2}$) and \hat{Q}_N (\hat{Q}_{N+2}) being the boson effective charge and the quadrupole operator, respectively, for the $[n]$ ($[n+2]$) space. The $E0$ operator is given as $\hat{T}(E0) = e_{0,n}^s\hat{n}_s + e_{0,n}^d\hat{n}_d$ for the $[n]$ space and the same expression for the $[n+2]$ space. The fixed effective charges $e_{0,n}^s = 0.7 \text{ efm}^2$ and $e_{0,n}^d = 1.3 \text{ efm}^2$ are employed for both configurations of the $N = 28$ isotones below $Z = 20$.

To complement the discussion, the NSM calculations for ^{42}Si , ^{44}S and ^{46}Ar , $N = 28$ isotones below ^{48}Ca are performed with the NushellX code [27] using the SDPF-MU interaction [11]. The full sd (pf) valence space is used for protons (neutrons). The center-of-mass correction is taken care of as default. The NSM calculations for ^{50}Ti , ^{52}Cr , and ^{54}Fe , $N = 28$ isotones above ^{48}Ca , and $^{42,44,46}\text{Ca}$ isotopes are performed with two fp -space interactions, GXPF1A [28] and KB3G [29].

2.1. Procedure of fitting the IBM-CM parameters

In Table 1, the parameters used in the IBM-CM calculations are listed. As noted above, to reduce the number of parameters, here we assume for the parameter χ the $\text{SU}(3)$ and $\overline{\text{SU}(3)}$ limits, $\chi = -1.33$ and 1.33 for the intruder configuration of ^{44}S , and for the normal configuration for ^{42}Si , respectively. In addition, the single d -boson energy for the \hat{n}_d term, a Casimir operator of nearly spherical $\text{U}(5)$ symmetry, generally has systematic of decreasing as a function of valence nucleon numbers [22]. Therefore, when ϵ is small, and the coefficients a_1 (for the $\hat{L} \cdot \hat{L}$ term) and a_2 (for the $\hat{Q} \cdot \hat{Q}$ term) are non-zero, with χ for the latter being -1.33 or 1.33 , the resulting nuclear structure corresponds to the strongly deformed prolate $[\text{SU}(3)]$, or oblate $[\overline{\text{SU}(3)}]$ shapes.

With this in mind, ϵ is generally determined to fit the systematic of the measured 2_1^+ energy level. For example, in ^{42}Si , ϵ for both the $[n]$ and $[n+2]$ configurations is relatively small, i.e., $\epsilon < 0.5 \text{ MeV}$, since the experimental 2_1^+ energy is about 0.7 MeV , while in ^{44}S and ^{46}Ar , ϵ is large for both configurations, $\epsilon > 1 \text{ MeV}$, as the observed 2_1^+ energy level is at about $1.4 - 1.5 \text{ MeV}$. For ^{44}S , the measured 0_2^+ level is very close in energy to that of the 2_1^+ state. To account for this nuclear structure, the intruder configuration for this nucleus is here considered to be of strongly deformed $\text{SU}(3)$ nature, with $\chi = -1.33$ and $\epsilon = 0 \text{ MeV}$, so that the calculated 0_2^+ energy level becomes sufficiently low.

For the other $N = 28$ isotones ^{50}Ti , ^{52}Cr and ^{54}Fe , the experimental 2_1^+ excitation energy is approximately $1.4 - 1.5 \text{ MeV}$, so we take the ϵ values to be more or less in that range for all these three nuclei, irrespective of whether ^{40}Ca or ^{48}Ca is chosen as the inert core. Also for these nuclei, there hardly appears to be any signature of strong deformation, hence the parameter χ is assumed to be zero. Only the competition between the moments of inertia generated by $\hat{L} \cdot \hat{L}$ and $\hat{Q} \cdot \hat{Q}$ terms seems to be responsible

for reproducing the experimental energy spectra. Their large ϵ 's hence represent the dominance of the \hat{n}_d term, which favors a spherical shape, over the other interaction terms. This is the case for the $N = 28$ isotones, except for ^{42}Si in both configurations, and ^{44}S in the $[n + 2]$ configuration.

In the $^{42,44,46}\text{Ca}$ isotopes, the fixed parameters $a_2 = -0.05$ MeV and $\chi = 0$ are considered for both configurations, except for the non-zero value $\chi = -1.0$ for the $[n + 2]$ space for ^{44}Ca , which is so chosen in order to achieve an agreement with data. This may be related to the suppressed location of the 2_1^+ level in the middle of $f_{7/2}$ orbital, that is, $(f_{7/2})^4$ configuration. The adopted value for the a_1 coefficient is also almost similar between ^{42}Ca and ^{46}Ca , corresponding to the two-particle and two-hole spectra of the $(f_{7/2})^2$ configuration. In ^{44}Ca , the situation is a bit different due to the fact that it is in the middle of the $f_{7/2}$ shell. The energy ϵ is relatively small in Ca isotopes, as compared to the $Z > 20$, $N = 28$ isotones, which are dominated by the $f_{7/2}$ orbital. This difference is due to the location of the 0_2^+ levels: In the $Z > 20$, $N = 28$ isotones, the 0_2^+ states are at higher excitation energy ranging from 2.6 – 3.8 MeV, while in the Ca isotopes, the 0_2^+ states are found at 1.8 MeV in $^{42,44}\text{Ca}$ and at 2.4 MeV in ^{46}Ca .

As regards the mixing interaction, we have assumed the same amount of the mixing strengths, α and β for a given nucleus, controlling the agreement of second-excited states and overall spectra. These mixing strength parameters could be different between the s and d boson parts, whereas in majority of the previous IBM-CM calculations the equal mixing strengths have been employed for realistic nuclear structure studies. The energy off-set Δ is fitted to mainly reproduce the location of the 0_2^+ level in all the chosen nuclei, but for ^{42}Si and ^{46}Ar . In the latter cases, experimental data are not available for the 0_2^+ excitation energies, and hence Δ is kept the same as that used in ^{44}S .

3. Results

First, the IBM-CM is applied to the $N = 28$ isotones ^{42}Si , ^{44}S and ^{46}Ar . The doubly-magic nucleus ^{48}Ca is assumed to be the inert core, and hence the corresponding boson numbers N for the normal configurations of ^{42}Si , ^{44}S and ^{46}Ar equal 3, 2, and 1, respectively. The predicted and experimental level schemes are compared in Fig. 1. Since the spectroscopic data for ^{42}Si and ^{46}Ar are limited, let us focus on ^{44}S as a benchmark case for the IBM-CM where 0_2^+ isomer is known.

As shown in Fig. 1(a), the present calculation that assumes the mixing of the U(5) and SU(3) configurations agree nicely with the experimental data for the low-lying spectra in ^{44}S . For this nucleus the optimal values of the mixing parameters and the energy offset turn out to be $\alpha = \beta = 0.2$ MeV, and $\Delta = 0.55$ MeV, respectively, as listed in Table 1. These parameter values are commonly used for the ^{42}Si and ^{46}Ar . Such an amount of mixing between the normal and intruder space configurations allows for the 0_2^+ to stay very near to the 2_1^+ state, leading to the isomeric nature of the 0_2^+ state. As shown in Fig. 2(a), the IBM-CM calculation suggests that the 0_1^+ and 0_2^+ states are

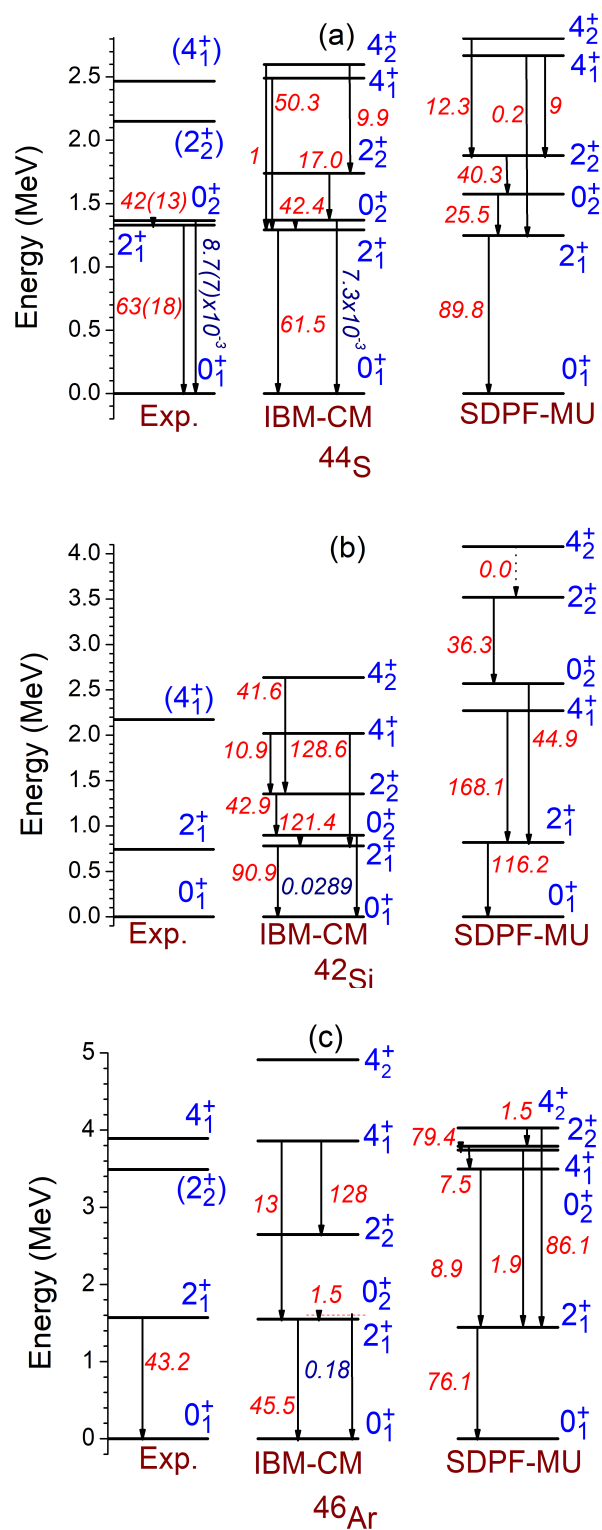


Figure 1. Comparison of the experimental [30], calculated level scheme for (a) ^{44}S , (b) ^{42}Si , and (c) ^{46}Ar . The $B(E2)$ values are shown in the units of $e^2\text{fm}^4$ as red italic numbers along the transition. The blue italic number denotes the $\rho^2(E0; 0_2^+ \rightarrow 0_1^+)$ values. NSM results based on SDPF-MU interaction are also shown.

mainly dominated by the $[n]$ U(5) and $[n + 2]$ SU(3) ones, respectively, thus indicating the shape coexistence. On the other hand, both normal and intruder configurations are equally mixed in the 2_1^+ state, with the probability of $\approx 50\%$, as depicted in Fig. 2(a). The yrast state, 4_1^+ , and yrare states, 2_2^+ and 4_2^+ , are again dominated by the deformed ($[n + 2]$) configuration. With the bosonic effective charges, $e_{2,n} = e_{2,n+2} = 5 e\text{fm}^2$, which are fitted to the observed $B(E2; 2_1^+ \rightarrow 0_1^+)$ values, the measured $B(E2; 0_2^+ \rightarrow 2_1^+)$ rate is reproduced reasonably. The calculated $\rho^2(E0)$ values for the $0_2^+ \rightarrow 0_1^+$ transition agree well with the experimental value. These results indicate an ability of the IBM-CM to describe quantitatively the low-lying states of ^{44}S and, especially, to give the implication for the 0_2^+ isomeric nature of this nucleus.

In ^{44}S , the present calculation suggests the 0_1^+ state to be primarily characterized by a spherical U(5) structure. This is explained by the parameters for the IBM-CM Hamiltonian used in calculations: the parameter $\chi = 0$, and ϵ is large, but there is no contributions from the $\hat{Q} \cdot \hat{Q}$ term, with the strength $a_2 = 0$ MeV for the $[n]$ configuration. The 0_2^+ isomer, on the other hand, is predominantly described by a rotor SU(3) structure, indicated by $\chi = -1.33$ and $\epsilon = 0$. This difference in the structure of wave function explains why the $E0$ transition between the 0_2^+ and 0_1^+ states involves a shape change, confirming the 0_2^+ as a shape isomer. The 2_1^+ state for ^{44}S is determined by a strong mixture between the $[n]$, U(5), and $[n + 2]$, SU(3) configurations. Therefore, a strong $E2$ transition connecting the 0_2^+ to 2_1^+ states also serves as a signature of a shape mixing. Such a configuration mixing has been obtained in previous IBM-CM calculations in heavy nuclei such as those in the Pb-Hg region [2, 24, 35, 36], in the neutron-rich $N \approx 60$ [26, 37] isotopes, in the $Z \approx 50$ region [38], and in the $N \approx Z \approx 40$ region [39], where shape coexistence is empirically supposed to occur. The current analysis suggests that the configuration mixing may play a role in lighter mass region as well.

A similar conclusion has been drawn for the nuclear structure of ^{44}S in the previous theoretical studies using different nuclear models, e.g., within the NSM [7] based on the SDPF-U interaction [31], and within the symmetry conserving configuration mixing (SCCM) [6]. The SCCM study [6], in particular, obtained nearly degenerate 0_2^+ and 2_1^+ states, but a larger $B(E2; 0_2^+ \rightarrow 2_1^+)$ than experimentally suggested. The present IBM-CM is able to reproduce the $B(E2; 0_2^+ \rightarrow 2_1^+)$ transition strength that is remarkably close to the experimental data, whereas the calculations from other theoretical approaches [7, 6, 5] predicted this transition rate to be rather far from the measured value. The NSM of Ref. [7] could not explain the $\rho^2(E0)$ values, while the SCCM calculation was successful in obtaining the measured order. The present NSM calculation using the SDPF-MU interaction predicts the $B(E2; 0_2^+ \rightarrow 2_1^+)$ rate of $25.5 e^2\text{fm}^4$, which underestimates the measured value of $42 \pm 13 e^2\text{fm}^4$. Effective charges are $e_\pi = 1.35$ and $e_\nu = 0.35$, as used in [32]. Results for other properties obtained from the NSM calculation are also compared in Fig. 1.

In Fig. 1(a), for ^{44}S the calculated excitation energy of the 4_1^+ state, which decays mainly to the 2_1^+ state, is in agreement with the observed 4_1^+ energy level, with the

Table 1. Parameters used for the present IBM-CM calculations. For the parameters ϵ , a_1 , a_2 , and χ those values corresponding to the normal $[n]$ and intruder $[n+2]$ spaces are shown.

| Nucleus | Core | ϵ (MeV) | | a_1 (MeV) | | a_2 (MeV) | | χ | | $\alpha = \beta$ (MeV) | Δ (MeV) |
|------------------|------------------|------------------|---------|-------------|---------|-------------|---------|--------|---------|------------------------|----------------|
| | | $[n]$ | $[n+2]$ | $[n]$ | $[n+2]$ | $[n]$ | $[n+2]$ | $[n]$ | $[n+2]$ | | |
| ^{42}Si | ^{48}Ca | 0.4 | 0.5 | 0.055 | 0.0 | -0.02 | +0.05 | 1.33 | 0.0 | 0.2 | 0.55 |
| ^{44}S | ^{48}Ca | 1.2 | 0.0 | 0.045 | 0.055 | 0.0 | 0.006 | 0.0 | -1.33 | 0.2 | 0.55 |
| ^{46}Ar | ^{48}Ca | 1.2 | 1.1 | 0.045 | 0.015 | 0.0 | 0.06 | 0.0 | 0.0 | 0.2 | 0.55 |
| ^{50}Ti | ^{48}Ca | 0.90 | 0.75 | 0.08 | -0.075 | -0.06 | 0.0 | 0.0 | 0.0 | 0.3 | 1.7 |
| ^{52}Cr | ^{48}Ca | 0.90 | 0.75 | 0.08 | -0.075 | -0.06 | 0.02 | 0.0 | 0.0 | 0.3 | 1.4 |
| ^{54}Fe | ^{48}Ca | 0.90 | 0.75 | 0.08 | -0.075 | -0.06 | -0.01 | 0.0 | 0.0 | 0.3 | 1.4 |
| ^{50}Ti | ^{40}Ca | 1.65 | 1.45 | -0.06 | 0.08 | 0.01 | 0.06 | 0.0 | 0.0 | 0.3 | 0.9 |
| ^{52}Cr | ^{40}Ca | 1.30 | 0.9 | -0.03 | 0.01 | -0.01 | 0.055 | 0.0 | 0.0 | 0.3 | 0.9 |
| ^{54}Fe | ^{40}Ca | 1.20 | 0.90 | 0.048 | -0.085 | -0.018 | 0.005 | 0.0 | 0.0 | 0.3 | 0.9 |
| ^{42}Ca | ^{40}Ca | 0.40 | 0.40 | 0.20 | -0.01 | -0.05 | -0.05 | 0.0 | 0.0 | 0.25 | 1.0 |
| ^{44}Ca | ^{40}Ca | 0.60 | 0.40 | 0.05 | -0.004 | -0.05 | -0.05 | 0.0 | -1.0 | 0.25 | 1.1 |
| ^{46}Ca | ^{40}Ca | 0.80 | 0.80 | 0.18 | -0.04 | -0.05 | -0.05 | 0.0 | 0.0 | 0.25 | 1.0 |

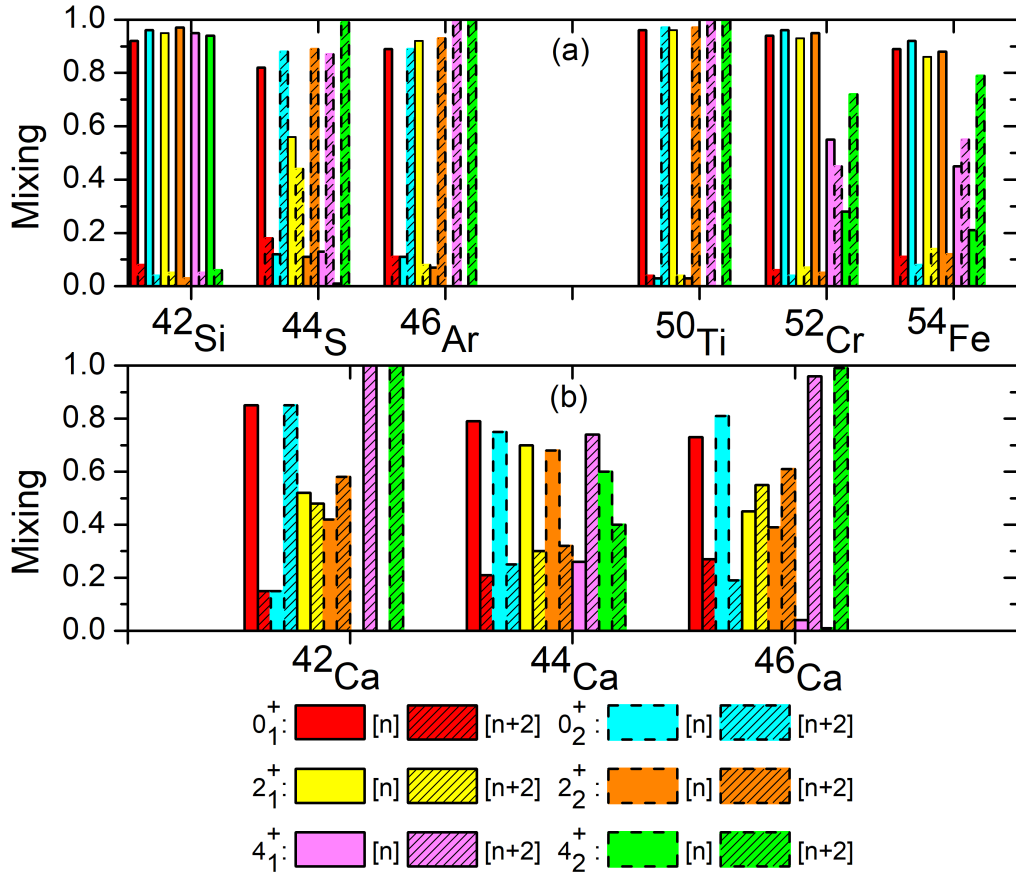


Figure 2. IBM-CM mixing amplitudes arising from both the $[n]$ and $[n+2]$ spaces for the low-lying yrast and yrare states in all the chosen nuclei.

spin and parity having not been firmly established. Furthermore, the IBM-CM predicts the energy ratio, $R_{4/2} = E(4_1^+)/E(2_1^+)$, to be $R_{4/2} < 2$ consistently with experiment.

Table 2. Average shell model proton and neutron-orbital occupancies for ^{42}Si , ^{44}S , and ^{46}Ar using SDPF-MU interaction.

| Nucleus | J^π | Protons | | | Neutrons | | | |
|------------------|---------|------------|------------|------------|------------|------------|------------|------------|
| | | $0d_{5/2}$ | $0d_{5/2}$ | $1s_{1/2}$ | $0f_{7/2}$ | $1p_{3/2}$ | $0f_{5/2}$ | $1p_{1/2}$ |
| ^{42}Si | 0_1^+ | 4.598 | 0.684 | 0.717 | 4.937 | 0.588 | 2.115 | 0.360 |
| | 0_2^+ | 4.931 | 0.613 | 0.455 | 5.854 | 0.447 | 1.371 | 0.328 |
| | 2_1^+ | 4.474 | 0.726 | 0.799 | 4.750 | 0.606 | 2.245 | 0.399 |
| | 2_2^+ | 4.605 | 0.854 | 0.540 | 5.383 | 0.367 | 1.756 | 0.493 |
| | 4_1^+ | 4.444 | 0.763 | 0.792 | 4.779 | 0.606 | 2.143 | 0.470 |
| | 4_2^+ | 4.960 | 0.570 | 0.469 | 5.764 | 0.404 | 1.511 | 0.320 |
| ^{44}S | 0_1^+ | 5.487 | 1.639 | 0.874 | 6.078 | 0.331 | 1.384 | 0.207 |
| | 0_2^+ | 5.547 | 1.662 | 0.790 | 5.889 | 0.271 | 1.290 | 0.549 |
| | 2_1^+ | 5.480 | 1.612 | 0.907 | 5.746 | 0.341 | 1.598 | 0.315 |
| | 2_2^+ | 5.398 | 1.658 | 0.943 | 5.687 | 0.321 | 1.716 | 0.275 |
| | 4_1^+ | 5.519 | 1.664 | 0.817 | 6.282 | 0.298 | 1.294 | 0.127 |
| | 4_2^+ | 5.567 | 1.532 | 0.899 | 5.450 | 0.344 | 1.699 | 0.506 |
| ^{46}Ar | 0_1^+ | 5.853 | 2.970 | 1.177 | 6.996 | 0.136 | 0.830 | 0.039 |
| | 0_2^+ | 5.888 | 3.010 | 1.102 | 6.341 | 0.146 | 1.372 | 0.142 |
| | 2_1^+ | 5.821 | 2.851 | 1.327 | 6.669 | 0.146 | 1.125 | 0.061 |
| | 2_2^+ | 5.782 | 2.741 | 1.477 | 6.199 | 0.184 | 1.529 | 0.088 |
| | 4_1^+ | 5.802 | 2.742 | 1.455 | 6.416 | 0.186 | 1.357 | 0.041 |
| | 4_2^+ | 5.771 | 2.808 | 1.421 | 6.123 | 0.169 | 1.412 | 0.296 |

Other theoretical calculations [6, 5], as well as the present NSM using the SDPF-MU interaction (see Fig. 1), could not reproduce this ratio. Within the IBM-CM, the 4_1^+ state is dominated by the $[n + 2]$ configuration, while in the 2_1^+ state two configurations are strongly mixed. This partly explains the measured energy ratio $R_{4/2} < 2$, and suggests the importance of the configuration mixing in the IBM framework, since with the usual *sd*-IBM space consisting of a single configuration, the calculated ratio $R_{4/2} \geq 2$.

Measurement of the $B(E2; 4_1^+ \rightarrow 2_1^+)$ transition in ^{44}S would shed more light upon this result. It is worth noting that the current analysis provides evidence for two 4^+ states in ^{44}S separated by an energy gap of 100 keV. The $B(E2; 4_1^+ \rightarrow 2_1^+)$ is about $50 e^2\text{fm}^4$, whereas the $B(E2; 4_2^+ \rightarrow 2_1^+)$ and $B(E2; 4_2^+ \rightarrow 2_2^+)$ are only $1 e^2\text{fm}^4$ and $10 e^2\text{fm}^4$, respectively. This observation conforms to the hypothesis of a low-lying 4^+ isomeric state in ^{44}S [33]. In the present calculation, the hindrance observed in the transition from the 4_2^+ state to 2_1^+ state can be comprehended by considering different bosonic spaces that are associated with different intrinsic shapes, see Fig. 2(a). The calculated 2_2^+ energy level looks a bit more suppressed than the tentatively assigned experimental one. Additionally, the 4_2^+ and 2_2^+ states are dominated by the $[n + 2]$ configuration. Although the 4_2^+ state could potentially be a longer-lived isomer, it does not qualify as a shape isomer. The IBM-CM suggests that for ^{44}S the 0p-0h and 2p-2h configurations are strongly mixed in the 2_1^+ state, while other states are relatively weakly

mixed, that is, they are accounted for by a pure normal or intruder configuration. This supports the weakening of $N = 28$ shell gap and broadening in nuclear wave functions beyond $f_{7/2}$ in the current shell model analysis as listed in Table 2, although the amount of core excitations can only be judged with full *sdpf*-NSM, which is beyond the scope of current study.

The low-lying level structure of ^{42}Si has been extensively investigated by experiments using new-generation radioactive-ion beams, such as the one at NSCL in 2019 [9]. In that reference, the two shell model interactions for the *sdpf* space, SDPF-MU [11] and SDPF-U-Si (SDPF-U valid for $Z \leq 14$) [31], could not conclude about the nature of the low-lying 0^+ excited states, especially the 0_2^+ state due to significantly different wave functions. The present IBM-CM calculation reproduces the low-lying yrast 2_1^+ and 4_1^+ states using the dominating (bosonic) $\overline{\text{SU}}(3)$ symmetry corresponding to oblate shape, which is assumed for the normal $[n]$ space. The 4_1^+ level has been tentatively assigned at 2.1 MeV experimentally. The calculated yrast and yrare states shown in Fig. 1(b) are dominated by the normal $[n]$ configuration in the IBM-CM.

Since the experimental yrast level scheme for ^{42}Si consisting of the 2_1^+ and 4_1^+ states looks like rotational band in Fig. 1(b), the IBM with single $\overline{\text{SU}}(3)$ configuration may appear to give a sufficiently good description for ^{42}Si , even without introducing the core excitation. Nevertheless, we perform the IBM-CM calculation, especially to identify the nature of the excited 0^+ and other yrare states. The bosonic effective charges $e_{2,n} = e_{2,n+2} = 5 \text{ efm}^2$ are used as in ^{44}S because the measured $B(E2; 2_1^+ \rightarrow 0_1^+)$ in ^{42}Si is not yet known. The effect of including the configuration mixing in this case is such that, the 0_2^+ state appears very close in energy to the 2_1^+ state. Similar results have been obtained from the NSM calculation with the SDPF-U-Si interaction in Ref. [9]. No experimental $B(E2)$ has been available for ^{42}Si , thus the mystery of the 0_2^+ state deserves further investigation by experiments using RI beams [34]. The inclusion of the configuration mixing in the IBM for ^{42}Si could also be supported by the self-consistent mean-field calculations within the Hartree-Fock-Bogoliubov (HFB) method that employed the Gogny-D1S energy density functional [16]. The triaxial quadrupole potential energy surface computed by the constrained Gogny-HFB calculation [17] suggested an oblate global minimum at $\beta \approx 0.35$ and a prolate secondary minimum with almost the same deformation. Furthermore more recent *ab initio* valence-space in-medium similarity renormalization group calculations [18] have provided a positive quadrupole moment $Q(2_1^+)$ for ^{42}Si , suggesting an oblate deformation. To conclude, in the IBM-CM for ^{42}Si , only the oblate $\overline{\text{SU}}(3)$ symmetry is assumed for the $[n]$ space with $\chi = 1.33$, while the $[n + 2]$ space with $\chi = 0$ and $a_1 = 0$ MeV indicates a nearly spherical symmetry. Configuration-mixing calculations have predicted a 0_2^+ isomer, considering the limited experimental data available, although this is subject to further measurements. The current analysis does not classify this as a shape isomer.

As for the ^{46}Ar nucleus, the calculated energy levels for the 2_1^+ and 0_2^+ states in the IBM-CM are found to be quite degenerate. One can see in Fig. 1(c) that the agreement between calculated energies and experimental data is reasonable. However, the yrast

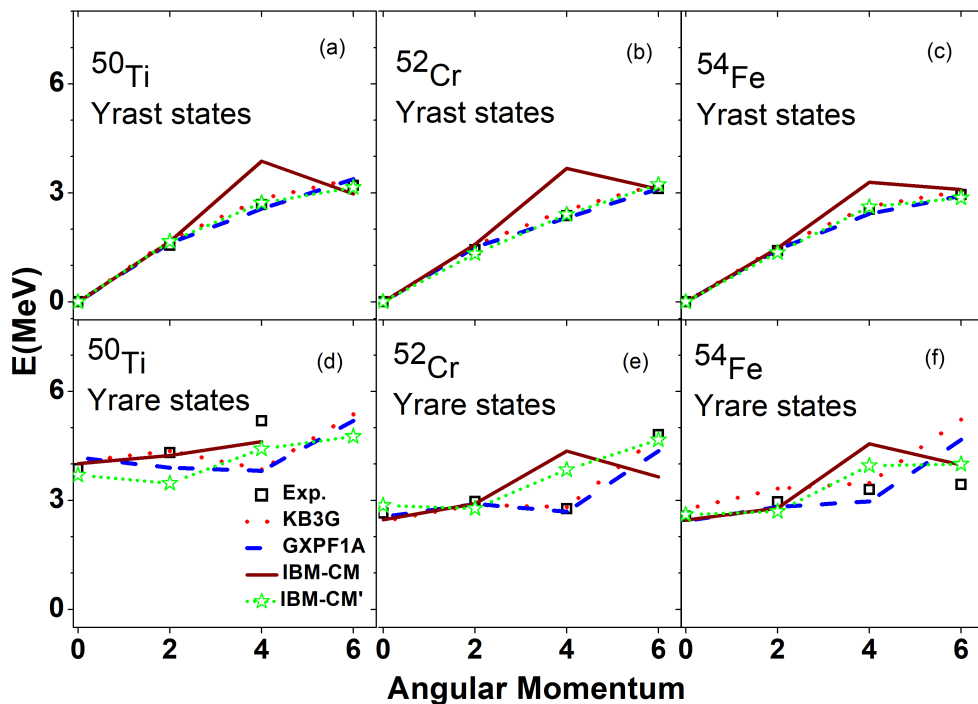


Figure 3. Comparison between the experimental [30] and calculated excitation energies for the $N = 28$ isotones. The NSM results using the KB3G and GXPF1A interactions are also shown.

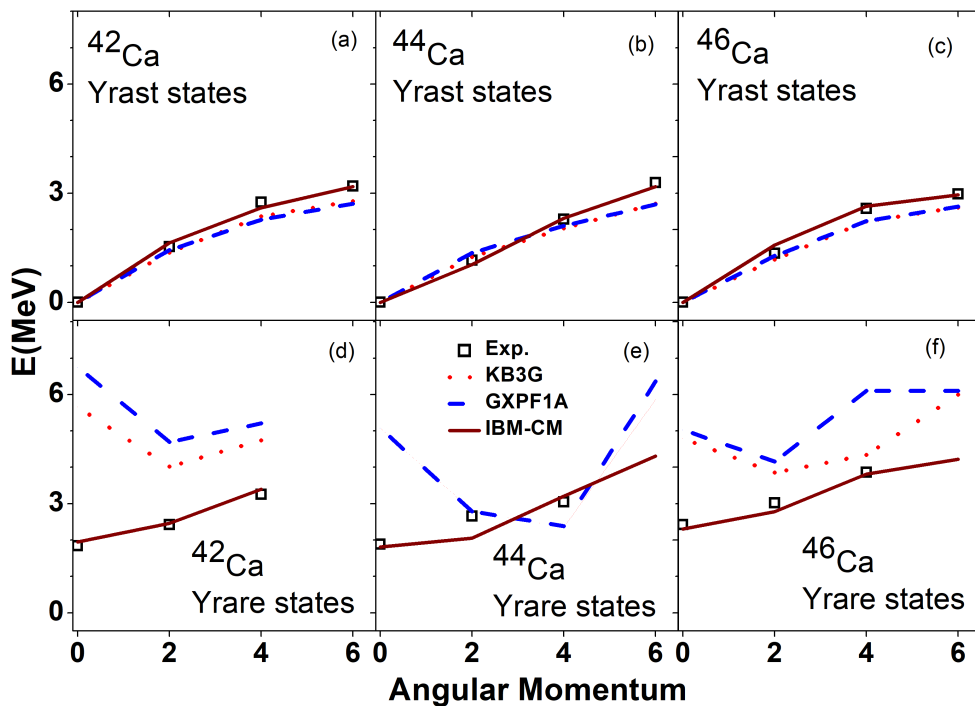


Figure 4. Same as Fig. 3 but for the $^{42,44,46}\text{Ca}$ isotopes.

states are expected to be of spherical in nature, as this nucleus is just one boson away from the doubly magic nucleus ^{48}Ca . The yrast states, 0_1^+ and 2_1^+ , in the IBM-CM are mainly dominated by the normal $[n]$ space, while the 4_1^+ , 0_2^+ , 2_2^+ , and 4_2^+ states by the intruder $[n+2]$ space. Only the $B(E2; 2_1^+ \rightarrow 0_1^+)$ is experimentally known, which is used to fit the bosonic effective charges as $e_{2,n} = e_{2,n+2} = 6 \text{ efm}^2$. The IBM-CM calculation suggests vanishing $B(E2; 4_2^+ \rightarrow 2_2^+)$ and $B(E2; 2_2^+ \rightarrow 0_2^+)$ values, but a substantially large $B(E2; 4_1^+ \rightarrow 2_2^+)$ rate. It would be of interest to reveal its (non)isomeric nature of the 0_2^+ state experimentally. The calculated 2_2^+ energy level is a bit more suppressed than that of the proposed 2_2^+ state in measured spectra. However, there is an energy level at 2.7 MeV in experiment with unidentified spin and parity, which is very close in energy to the 2_2^+ state predicted by the IBM-CM. This may encourage further experimental investigation. In summary, for ^{46}Ar , the chosen parameters, characterized by the large ϵ values in both the $[n]$ and $[n+2]$ spaces, suggest a spherical structure, as compared to ^{44}S and ^{42}Si . Nevertheless, the IBM-CM calculations also suggest a 0_2^+ isomer, but it would not be a shape isomer. The transition from 0_2^+ to 0_1^+ would be hindered by the change in the dominant space and resulting nucleonic configurations.

Figure 3(a)-(f) compares the experimental and calculated energy spectra of both the yrast and yrare 0^+ , 2^+ , 4^+ , and 6^+ states for the $N = 28$ isotones, ^{50}Ti , ^{52}Cr , and ^{54}Fe . The IBM-CM calculation is performed with the inert core ^{48}Ca . The agreement between the IBM-CM and experimental energies is reasonable for the yrast states, except for 4_1^+ states. It is due to the limited number of bosons, and could be remedied if one takes the ^{40}Ca doubly-magic nucleus as the inert core for these isotones. The IBM-CM description of the yrare states, 0_2^+ and 2_2^+ , is also reasonable. These isotones are assumed to be nearly spherical in the present calculation. However, core excitations would make a non-negligible contribution to the low-lying states. Note that the Gogny-HFB calculation for the studied $N = 28$ isotones exhibit a flat-bottomed potential with a spherical minimum [16], in particular, for the nucleus ^{52}Cr . Figure 3 further depicts the NSM results on the excitation energies using the KB3G and GXPF1A interactions. The NSM explains both the yrast and yrare states of these isotonic nuclei well, and also supports the spread in neutron wave functions beyond the $f_{7/2}$ shell, especially for the yrare states as listed in Table 3. This conclusion is compatible with the IBM-CM interpretation.

In $N = 28$ isotones with $Z > 20$, a nearly spherical structure is assumed in IBM-CM. Given the assumption of a ^{48}Ca core with the frozen neutron $f_{7/2}$ orbitals, calculations using a limited number of bosons fail to accurately reproduce the measured 4^+ state with the simple IBM-1 Hamiltonian and the chosen interaction strengths. Comparative NSM analysis with fp -shell interactions also showed that the low-lying levels did not support the average occupancies of neutron $f_{7/2}$ as frozen listed in Table 3. Consequently, further analysis was conducted by assuming ^{40}Ca as an IBM-CM core, denoted as IBM-CM' in Fig. 3, which better explain the spectra for these nuclei, including the 4^+ states. The results with a larger number of bosons with ^{40}Ca core suggest that the low-lying states in these $N = 28$ isotonic nuclei require to include the

neutron $f_{7/2}$ as an active orbital.

A similar comparison is made for the low-lying yrast and yrare state excitations of $^{42,44,46}\text{Ca}$ isotopes in Figs. 4(a)-(f). In this case, ^{40}Ca is adopted as the inert core for the IBM-CM. The IBM-CM reproduces the measured energy spectra of both the yrast and yrare states quite well. The NSM with the two fp -shell interactions, KB3G and GXPF1A, also explain the yrast states, but stay very far from the experimental data for yrare states. The average occupancies of active neutron shell model orbitals are listed in Table 4. The IBM-CM results clearly signify the importance of core excitations, or intruder states, for the description of yrare states. However, the NSM calculation with the fp -shell interactions could not directly support this finding. This is due to the use of ^{40}Ca as the inert core and, to correctly describe the measured systematic of those second-excited yrare bands, particle-hole excitations from the sd to pf shells would have to be taken into account. Such an extension would be, however, computationally highly demanding [40].

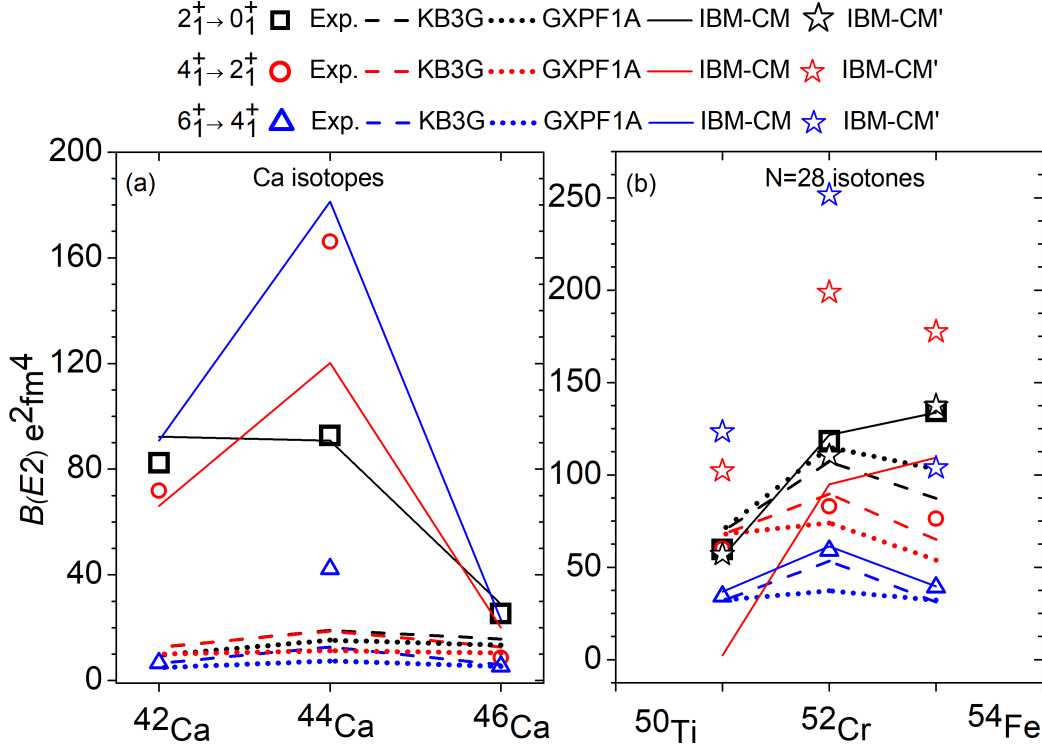


Figure 5. Comparison of the experimental [30] and calculated $B(E2; I \rightarrow I - 2)$ values for (a) the $^{42,44,46}\text{Ca}$ isotopes, and for (b) the ^{50}Ti , ^{52}Cr and ^{54}Fe , $N = 28$ isotones. In NSM (based on GXPF1A and KB3G), the effective neutron (proton) charge $e_\nu = 0.65$ ($e_\pi = 1.3$) is used for the Ca isotopes ($N = 28$ isotones).

Figure 5 compares the experimental [30] and calculated $B(E2; I \rightarrow I - 2)$ transition rates for (a) the $^{42,44,46}\text{Ca}$ isotopes, and (b) the $N = 28$ isotones ^{50}Ti , ^{52}Cr and ^{54}Fe . The bosonic effective charges $(e_{2,n}, e_{2,n+2}) = (10.0, 5.5)$, $(5.5, 5.5)$, and $(3.5, 1.5)$ for $^{42,44,46}\text{Ca}$ isotopes, respectively, and $(e_{2,n}, e_{2,n+2}) = (7.5, 3.5)$, $(7.5, 4.5)$, and $(6.5, 2.3)$ for ^{50}Ti ,

Table 3. Average shell model proton and neutron-orbital occupancies for ^{50}Ti , ^{52}Cr and ^{54}Fe , $N=28$ isotonic nuclei from GXPF1A and KB3G interactions.

| Nucleus | J^π | Interaction | Protons | | | | Neutrons | | | | |
|------------------|------------------|-------------|------------|------------|------------|------------|------------|------------|------------|------------|-------|
| | | | $0f_{7/2}$ | $1p_{3/2}$ | $0f_{5/2}$ | $1p_{1/2}$ | $0f_{7/2}$ | $1p_{3/2}$ | $0f_{5/2}$ | $1p_{1/2}$ | |
| ^{50}Ti | 0_1^+ | GXPF1A | 1.915 | 0.049 | 0.031 | 0.006 | 7.573 | 0.238 | 0.139 | 0.050 | |
| | | KB3G | 1.829 | 0.044 | 0.112 | 0.015 | 7.499 | 0.219 | 0.227 | 0.055 | |
| | 0_2^+ | GXPF1A | 1.839 | 0.120 | 0.025 | 0.016 | 6.031 | 1.496 | 0.256 | 0.217 | |
| | | KB3G | 1.734 | 0.166 | 0.075 | 0.025 | 5.759 | 1.572 | 0.331 | 0.338 | |
| | 2_1^+ | GXPF1A | 1.923 | 0.060 | 0.012 | 0.004 | 7.445 | 0.362 | 0.138 | 0.054 | |
| | | KB3G | 1.895 | 0.053 | 0.042 | 0.010 | 7.415 | 0.304 | 0.223 | 0.057 | |
| | 2_2^+ | GXPF1A | 1.839 | 0.123 | 0.026 | 0.013 | 6.716 | 1.036 | 0.154 | 0.094 | |
| | | KB3G | 1.812 | 0.085 | 0.082 | 0.020 | 6.566 | 1.088 | 0.244 | 0.102 | |
| | 4_1^+ | GXPF1A | 1.927 | 0.046 | 0.020 | 0.007 | 7.542 | 0.252 | 0.143 | 0.063 | |
| | | KB3G | 1.900 | 0.042 | 0.044 | 0.014 | 7.481 | 0.235 | 0.224 | 0.060 | |
| | 4_2^+ | GXPF1A | 1.836 | 0.123 | 0.028 | 0.013 | 6.735 | 0.982 | 0.189 | 0.094 | |
| | | KB3G | 1.801 | 0.095 | 0.085 | 0.020 | 6.660 | 1.002 | 0.246 | 0.091 | |
| | 6_1^+ | GXPF1A | 1.936 | 0.025 | 0.035 | 0.004 | 7.675 | 0.171 | 0.118 | 0.036 | |
| | | KB3G | 1.914 | 0.019 | 0.061 | 0.006 | 7.586 | 0.158 | 0.213 | 0.043 | |
| | 6_2^+ | GXPF1A | 1.865 | 0.099 | 0.026 | 0.010 | 6.640 | 1.085 | 0.177 | 0.098 | |
| | | KB3G | 1.868 | 0.075 | 0.042 | 0.015 | 6.575 | 1.089 | 0.236 | 0.100 | |
| | ^{52}Cr | 0_1^+ | GXPF1A | 3.747 | 0.118 | 0.119 | 0.016 | 7.436 | 0.293 | 0.214 | 0.057 |
| | | | KB3G | 3.634 | 0.093 | 0.243 | 0.030 | 7.373 | 0.245 | 0.319 | 0.063 |
| 0_2^+ | | GXPF1A | 3.376 | 0.461 | 0.114 | 0.049 | 5.814 | 1.118 | 0.649 | 0.419 | |
| | | KB3G | 3.454 | 0.334 | 0.169 | 0.043 | 5.707 | 1.171 | 0.633 | 0.488 | |
| 2_1^+ | | GXPF1A | 3.706 | 0.177 | 0.097 | 0.019 | 7.286 | 0.412 | 0.232 | 0.070 | |
| | | KB3G | 3.669 | 0.130 | 0.170 | 0.031 | 7.264 | 0.326 | 0.333 | 0.077 | |
| 2_2^+ | | GXPF1A | 3.530 | 0.339 | 0.092 | 0.039 | 6.484 | 0.786 | 0.462 | 0.268 | |
| | | KB3G | 3.467 | 0.332 | 0.157 | 0.043 | 5.829 | 1.069 | 0.635 | 0.467 | |
| 4_1^+ | | GXPF1A | 3.720 | 0.153 | 0.110 | 0.016 | 7.356 | 0.355 | 0.222 | 0.067 | |
| | | KB3G | 3.695 | 0.133 | 0.146 | 0.025 | 7.299 | 0.303 | 0.324 | 0.075 | |
| 4_2^+ | | GXPF1A | 3.785 | 0.144 | 0.053 | 0.018 | 7.233 | 0.436 | 0.274 | 0.057 | |
| | | KB3G | 3.767 | 0.087 | 0.119 | 0.026 | 7.311 | 0.306 | 0.325 | 0.058 | |
| 6_1^+ | | GXPF1A | 3.838 | 0.086 | 0.067 | 0.010 | 7.507 | 0.259 | 0.184 | 0.049 | |
| | | KB3G | 3.780 | 0.066 | 0.136 | 0.018 | 7.449 | 0.203 | 0.294 | 0.055 | |
| 6_2^+ | | GXPF1A | 3.536 | 0.320 | 0.108 | 0.036 | 6.540 | 0.896 | 0.392 | 0.172 | |
| | | KB3G | 3.583 | 0.224 | 0.154 | 0.040 | 6.526 | 0.899 | 0.406 | 0.169 | |
| ^{54}Fe | | 0_1^+ | GXPF1A | 5.621 | 0.190 | 0.164 | 0.026 | 7.431 | 0.293 | 0.225 | 0.051 |
| | | | KB3G | 5.524 | 0.124 | 0.313 | 0.039 | 7.398 | 0.199 | 0.346 | 0.056 |
| | 0_2^+ | GXPF1A | 5.250 | 0.493 | 0.191 | 0.066 | 5.797 | 1.141 | 0.653 | 0.409 | |
| | | KB3G | 5.314 | 0.341 | 0.285 | 0.059 | 5.635 | 1.243 | 0.619 | 0.503 | |
| | 2_1^+ | GXPF1A | 5.586 | 0.253 | 0.132 | 0.029 | 7.313 | 0.388 | 0.238 | 0.060 | |
| | | KB3G | 5.579 | 0.156 | 0.226 | 0.039 | 7.353 | 0.242 | 0.345 | 0.060 | |
| | 2_2^+ | GXPF1A | 5.165 | 0.533 | 0.234 | 0.069 | 6.421 | 0.933 | 0.430 | 0.217 | |
| | | KB3G | 5.304 | 0.360 | 0.276 | 0.060 | 5.699 | 1.155 | 0.650 | 0.495 | |
| | 4_1^+ | GXPF1A | 5.698 | 0.161 | 0.117 | 0.025 | 7.438 | 0.288 | 0.224 | 0.051 | |
| | | KB3G | 5.652 | 0.105 | 0.208 | 0.035 | 7.432 | 0.184 | 0.330 | 0.054 | |
| | 4_2^+ | GXPF1A | 5.424 | 0.354 | 0.177 | 0.045 | 6.616 | 0.857 | 0.357 | 0.170 | |
| | | KB3G | 5.430 | 0.230 | 0.287 | 0.053 | 6.539 | 0.907 | 0.379 | 0.176 | |
| | 6_1^+ | GXPF1A | 5.727 | 0.149 | 0.107 | 0.017 | 7.508 | 0.251 | 0.200 | 0.041 | |
| | | KB3G | 5.673 | 0.098 | 0.201 | 0.028 | 7.461 | 0.166 | 0.325 | 0.049 | |
| | 6_2^+ | GXPF1A | 5.382 | 0.392 | 0.176 | 0.050 | 6.514 | 0.700 | 0.673 | 0.113 | |
| | | KB3G | 5.389 | 0.237 | 0.321 | 0.053 | 6.610 | 0.394 | 0.878 | 0.118 | |

^{52}Cr and ^{54}Fe , respectively, are obtained from the fit to the $B(E2; 2_1^+ \rightarrow 0_1^+)$ value for each nucleus. The different bosonic effective charges between the two configurations are

Table 4. Average shell model neutron-orbital occupancies for $^{42,44,46}\text{Ca}$ from GXPF1A and KB3G interactions.

| Nucleus | J^π | GXPF1A | | | | KB3G | | | |
|------------------|---------|------------|------------|------------|------------|------------|------------|------------|------------|
| | | $0f_{7/2}$ | $1p_{3/2}$ | $0f_{5/2}$ | $1p_{1/2}$ | $0f_{7/2}$ | $1p_{3/2}$ | $0f_{5/2}$ | $1p_{1/2}$ |
| ^{42}Ca | 0_1^+ | 1.945 | 0.031 | 0.019 | 0.005 | 1.846 | 0.062 | 0.074 | 0.018 |
| | 0_2^+ | 0.042 | 1.762 | 0.028 | 0.169 | 0.083 | 1.798 | 0.002 | 0.117 |
| | 2_1^+ | 1.965 | 0.032 | 0.002 | 0.001 | 1.914 | 0.068 | 0.011 | 0.007 |
| | 2_2^+ | 0.989 | 0.976 | 0.014 | 0.021 | 1.032 | 0.940 | 0.013 | 0.015 |
| | 4_1^+ | 1.977 | 0.014 | 0.005 | 0.003 | 1.953 | 0.028 | 0.010 | 0.009 |
| | 4_2^+ | 1.010 | 0.938 | 0.008 | 0.044 | 1.022 | 0.902 | 0.013 | 0.063 |
| | 6_1^+ | 1.991 | 0.000 | 0.009 | 0.000 | 1.985 | 0.000 | 0.015 | 0.000 |
| | 6_2^+ | 1.009 | 0.000 | 0.991 | 0.000 | 1.015 | 0.000 | 0.985 | 0.000 |
| ^{44}Ca | 0_1^+ | 3.889 | 0.057 | 0.046 | 0.009 | 3.756 | 0.090 | 0.129 | 0.026 |
| | 0_2^+ | 2.893 | 1.068 | 0.021 | 0.018 | 2.761 | 1.153 | 0.048 | 0.038 |
| | 2_1^+ | 3.895 | 0.076 | 0.024 | 0.005 | 3.806 | 0.108 | 0.067 | 0.018 |
| | 2_2^+ | 3.895 | 0.083 | 0.010 | 0.011 | 3.833 | 0.115 | 0.028 | 0.025 |
| | 4_1^+ | 3.888 | 0.073 | 0.035 | 0.004 | 3.834 | 0.109 | 0.046 | 0.011 |
| | 4_2^+ | 3.948 | 0.037 | 0.010 | 0.005 | 3.885 | 0.050 | 0.050 | 0.015 |
| | 6_1^+ | 3.948 | 0.025 | 0.024 | 0.003 | 3.892 | 0.037 | 0.061 | 0.010 |
| | 6_2^+ | 2.938 | 0.956 | 0.041 | 0.064 | 2.919 | 0.959 | 0.044 | 0.078 |
| ^{46}Ca | 0_1^+ | 5.886 | 0.074 | 0.050 | 0.010 | 5.738 | 0.092 | 0.143 | 0.026 |
| | 0_2^+ | 4.906 | 1.041 | 0.032 | 0.021 | 4.870 | 1.026 | 0.069 | 0.035 |
| | 2_1^+ | 5.867 | 0.097 | 0.030 | 0.006 | 5.791 | 0.108 | 0.082 | 0.019 |
| | 2_2^+ | 4.904 | 1.011 | 0.051 | 0.033 | 4.790 | 1.033 | 0.105 | 0.072 |
| | 4_1^+ | 5.912 | 0.052 | 0.028 | 0.008 | 5.839 | 0.067 | 0.074 | 0.020 |
| | 4_2^+ | 4.915 | 0.989 | 0.068 | 0.028 | 4.832 | 1.014 | 0.111 | 0.043 |
| | 6_1^+ | 5.924 | 0.043 | 0.029 | 0.004 | 5.856 | 0.055 | 0.075 | 0.014 |
| | 6_2^+ | 4.929 | 1.004 | 0.049 | 0.018 | 4.876 | 0.980 | 0.081 | 0.063 |

considered here, which are determined so as to account for the mixing amplitudes of the normal $[n]$ and intruder $[n + 2]$ bosonic spaces in the 0_1^+ and 2_1^+ states, as plotted in Fig. 2(a) for ^{50}Ti , ^{52}Cr and ^{54}Fe isotones, and Fig. 2(b) for $^{42,44,46}\text{Ca}$ isotopes. The larger value of $[n]$ space effective charge reflects the dominance of normal configuration for the states in the given transition. The $B(E2)$ estimates with ^{40}Ca core, IBM-CM' are also shown with stars in Fig. 5(b) using the bosonic effective charges $(e_{2,n}, e_{2,n+2}) = (3.8, 0.9)$, $(4.7, 0.7)$, and $(5.0, 1.5)$, for ^{50}Ti , ^{52}Cr and ^{54}Fe , respectively. One can judge the dominance of $[n]$ configuration in IBM-CM' set from the used effective charges, as should be the case with ^{40}Ca core for $Z > 20$, $N = 28$ isotones, since we have already included below the core-excitations by shifting the core for these isotones. For the Ca isotopes, the predicted $B(E2; 4_1^+ \rightarrow 2_1^+)$ transitions are close to the measured ones, but the $B(E2; 6_1^+ \rightarrow 4_1^+)$ rates are considerably overestimated. In the $N = 28$ isotones, the $B(E2)$ values computed with the IBM-CM, in most cases, agree with the experimental data. A discrepancy is found for the $4_1^+ \rightarrow 2_1^+$ transition in ^{50}Ti . This could be corrected by using a larger number of bosons. The fp -shell model results are in reasonable agreement for the yrast level scheme in $Z > 20$, $N = 28$ isotones; ^{50}Ti ,

^{52}Cr and ^{54}Fe . Though the yrare states do not support $f_{7/2}$ as fully filled, i.e. $N = 28$ subshell closure, as can be followed from the average occupancies listed in Table 3. The IBM-CM analysis provides a consistent result.

The NSM prediction on the $B(E2)$ values, for both the KB3G and GXPF1A effective interactions, underestimates the data for the Ca isotopes, but is in a reasonable agreement with data for the $N = 28$ isotones. The 6_1^+ isomeric nature in the isotonic nuclei, ^{50}Ti and ^{54}Fe , is very well explained by the NSM based on the two interactions. For ^{52}Cr , there are two 4^+ states lying close to each other, providing an extra decay branch for the 6_1^+ state and no isomer.

For the $^{42,44,46}\text{Ca}$ isotopes, the IBM-CM results suggest the importance of core excitations. This is also evident in the fp -shell model results, based on both the GXPF1A and KB3G interactions, which are not sufficient in explaining the transition probabilities between the yrast levels (cf. Fig. 5). The incorporation of core excitations in IBM is relatively feasible as compared to the NSM, even for lighter mass nuclei.

4. Conclusions

Structure of ^{42}Si , ^{44}S , and ^{46}Ar has been studied in terms of the IBM-CM, which has rarely been applied in light-mass regions. The nature of ^{42}Si has been attributed to be of deformed, $\text{SU}(3)$, character. The interpretation within the IBM-CM that the 0_2^+ (shape) isomer in ^{44}S arises from the shape coexistence provides a crucial piece of knowledge about the shape isomers across the nuclear landscape, which remains an open issue in nuclear structure physics. ^{46}Ar is shown to be nearly spherical, but the nature of the 0_2^+ state deserves further investigations by experiment. The fp -shell shell model calculations are in a reasonable agreement for the yrast level scheme in $Z > 20$, $N = 28$ isotones; ^{50}Ti , ^{52}Cr and ^{54}Fe . Though the yrare states do not support $f_{7/2}$ as fully filled, i.e. $N=28$ subshell closure, as can be followed from the average occupancies listed in Table 3. This finding is consistent with that of the IBM-CM analysis. Structure of the $N = 28$ isotones above ^{48}Ca differs significantly from those nuclei below $Z = 20$, even though both regions are sensitive to core excitations. The IBM-CM calculation for $^{42,44,46}\text{Ca}$ isotopes sheds light upon the interpretation of their yrare states and transition probabilities between the yrast states.

This work will pave a way to study nuclear structure properties in this mass region which are of much interest for future measurements. For instance, these results on the shell-breaking mechanism at the first spin-orbit closed shell $N = 28$ are relevant for charge radii puzzle around ^{48}Ca [41]. In addition, it is also of crucial importance to assess the suitability of the IBM-CM consisting of the collective s and d bosons for the interpretation of the low-lying states of light nuclei, especially for those in which seniority-type configurations are expected to play a dominant role. This could be addressed by analyzing the IBM-CM wave functions in connection to the underlying shell structure, or including additional degrees of freedom beyond s and d ones. These analyses present an interesting future work.

5. Acknowledgements

The author BM gratefully acknowledges the financial support from the Croatian Science Foundation and the École Polytechnique Fédérale de Lausanne, under the project TTP-2018-07-3554 “Exotic Nuclear Structure and Dynamics”, with funds of the Croatian-Swiss Research Programme.

- [1] M. Goeppert-Mayer and J. H. D. Jensen, *Elementary theory of nuclear shell structure* (Wiley, New York, 1955).
- [2] K. Heyde, and J.L. Wood Rev. Mod. Phys. **83**, 1467 (2011).
- [3] B. Bastin *et al.*, Phys. Rev. Lett. **99**, 022503 (2007).
- [4] T. Otsuka, A. Gade, O. Sorlin, T. Suzuki, Y. Utsuno, Rev. Mod. Phys. **92**, 015002 (2020).
- [5] D. Santiago-Gonzalez *et al.*, Phys. Rev. C **83**, 061305 (R) (2011).
- [6] Tomas R. Rodriguez and J. L. Egido, Phys. Rev. C **84**, 051307(R) (2011).
- [7] C. Force *et al.*, Phys. Rev. Lett. **105**, 102501 (2010).
- [8] S. Garg, B. Maheshwari, B. Singh, Y. Sun, A. Goel, and A. K. Jain, Atomic Data and Nuclear Data Tables **150**, 101546 (2023); A. K. Jain, B. Maheshwari, S. Garg, M. Patial, and B. Singh, Nucl. Data Sheets **128**, 1 (2015).
- [9] A. Gade *et al.*, Phys. Rev. Lett. **122**, 222501 (2019).
- [10] A.P. Zuker, J. Retamosa, A. Poves, and E. Caurier, Phys. Rev. C **52**, R1741 (1995).
- [11] Y. Utsuno, T. Otsuka, B. A. Brown, M. Honma, T. Mizusaki, and N. Shimizu, Phys. Rev. C **86**, 051301 (R) (2012).
- [12] T. Nomura, C. Gil, H. Saito, T. Yamazaki, and M. Ishihara, Phys. Rev. Lett. **25**, 1342 (1970).
- [13] R. Hensler, J. W. Tape, N. Benczer-Koller, and Jack R. MacDonald, Phys. Rev. Lett. **27**, 1587 (1971).
- [14] B. Maheshwari and K. Nomura, Symmetry **14**, 2680 (2022).
- [15] T. Mizusaki, T. Otsuka, M. Honma, and B. A. Brown, Phys. Rev. C **63**, 044306 (2001).
- [16] J.-P. Delaroche, M. Girod, J. Libert, H. Goutte, S. Hilaire, S. Péru, N. Pillet, and G. F. Bertsch, Phys. Rev. C **81**, 014303 (2010).
- [17] https://www-phynu.cea.fr/science_en_ligne/carte_potentiels_microscopiques/carte_potentiel_nucleaire_eng.htm
- [18] Q. Yuan, J.G. Li, and H.H. Li, Phys. Lett. B **848**, 138331 (2024).
- [19] P. Van Isacker, IBM-1 code, unpublished.
- [20] A. Arima and F. Iachello Phys. Rev. Lett. **35**, 1069 (1975).
- [21] A. Bohr and B.R. Mottelson, *Nuclear Structure*. Vol. II. Nuclear Deformations, (Benjamin, NY, 1975).
- [22] A. Arima and F. Iachello, *The interacting boson model* (Cambridge University Press, 1987).
- [23] T. Otsuka, A. Arima, and F. Iachello, Nucl. Phys. A **309**, 1 (1978).
- [24] P.D. Duval, and B.R. Barrett, Phys. Lett. B, **100(3)**, 223 (1981).
- [25] J. Jolie, R.F. Casten, P. von Brentano, and V. Werner, Phys. Rev. Lett. **87**, 162501 (2001).
- [26] M. Sambataro, G. Molnár, Nucl. Phys. A **376**, 201 (1982).
- [27] B. A. Brown, and W. D. M. Rae, Nucl. Data Sheets **120**, 115 (2014).
- [28] M. Honma, T. Otsuka, B. A. Brown and T. Mizusaki, Phys. Rev. C **65**, 061301(R) (2002); Euro. Phys. Jour. A **25**, 499 (2005).
- [29] A. Poves, J. Sanchez-Solano, E. Caurier, and F. Nowacki, Nucl. Phys. A **694**, 157 (2001).
- [30] Evaluated Nuclear Structure Data File, <https://www.nndc.bnl.gov/ensdf/>; Experimental Unevaluated Nuclear Data List, <https://www.nndc.bnl.gov/ensdf/xundl/index.jsp>.
- [31] F. Nowacki and A. Poves, Phys. Rev. C **79**, 014310 (2009).
- [32] R. Chevrier and L. Gaudefroy, Phys. Rev. C **89**, 051301(R) (2014).
- [33] J. J. Parker IV *et al.*, Phys. Rev. Lett. **118**, 052501 (2017).
- [34] H. L. Crawford *et al.*, Phys. Rev. Lett. **129**, 212501 (2022).

- [35] K. Nomura, et al., Phys. Rev. C **87**, 064313 (2013).
- [36] K. Nomura, T. Otsuka, P. Van Isacker, Jour. of Phys. G: Part. and Nucl. Phys. **43**, 024008 (2016).
- [37] K. Nomura, et al., Phys. Rev. C **94**, 044314 (2016).
- [38] A. Leviatan, et al., Phys. Rev. C **98**, 031302(R) (2018).
- [39] K. Nomura, Phys. Rev. C **106**, 024330 (2022).
- [40] E. Caurier, J. Menéndez, F. Nowacki, and A. Poves, Phys. Rev. C **75**, 054317 (2007).
- [41] R. F. Garcia Ruiz *et al.*, Nat. Phys. **12**, 594 (2016).